CHINESE OPTICS LETTERS

Vol. 20, No. 11 | November 2022

Interactions of the second-order solitons with an external probe pulse in the optical event horizon

Jifang Rong (荣继芳)[1], Yiwu Ma (马亿昨)[1], Meng Xu (徐 蒙)[2**], and Hua Yang (杨 华)[1*]

[1] College of Computer Science and Electronic Engineering, Hunan University, Changsha 410082, China

[2] School of Geosciences and Info-Physics, Central South University, Changsha 410083, China

*Corresponding author: huayang@hnu.edu.cn

**Corresponding author: xumeng@csu.edu.cn

Received April 5, 2022 | Accepted June 10, 2022 | Posted Online July 13, 2022

We demonstrate manipulating the interactions of a second-order soliton with a weak probe pulse under the condition of group velocity match and group velocity mismatch (GVMM). During these interactions, the second-order soliton acting as an effective periodic refractive-index barrier leads to the polychromatic scattering of the probe pulse, which is represented as unequally spaced narrow-band sources with adjustable spectral width. In the case of GVMM, almost all the spectral components of the narrow-band sources meet the nonlinear frequency conversion relationship by using the wavenumber-matching relationship due to the robustness of the second-order soliton under moderate high-order-dispersion perturbations, so this case is more conducive to the study of the soliton wells. In addition, different transmission states of a soliton well are demonstrated under different probe pulse properties in the fiber-optical analog of the event horizon. When the power of the probe pulse is strong enough, a dispersive wave can be generated from the collision of two fundamental solitons split from the two second-order solitons. These interesting phenomena investigated in this work as a combination of white- and black-hole horizons can be considered as promising candidates for frequency conversion and broadband supercontinuum generation.

Keywords: second-order soliton well; probe wave; optical event horizon.

DOI: 10.3788/COL202220.111901

1. Introduction

Solitons are localized nonlinear waves formed by a balance between dispersion and nonlinear effects and have broad applications in many physical systems including nonlinear fiber-optics[1], plasmas physics[2,3], fluid mechanics[4], and so on. These pulses exhibit similar characteristics, such as periodicity, particle-like property, as well as stability[1]. But they are sensitive to high-order dispersion (HOD) and nonlinear perturbation, which induce the split of higher-order solitons[5–10]. The soliton fission dynamics has been previously studied under the perturbations of self-steepening (SS), HOD, and stimulated Raman scattering, where a series of fundamental solitons with different group velocities as well as phase-matched dispersive waves (DWs) are generated[11–13]. Therefore, high-order soliton fission is a crucial mechanism responsible for producing ultrashort frequency-shifted fundamental solitons and ultra-broadband supercontinuum (SC).

As one of the vital physical mechanisms for ultra-broadband SC generation, the interaction between fundamental solitons and DWs in nonlinear waveguides has been thoroughly studied in the past decade[6,13]. When a relatively weak probe wave transmits along with an energetic soliton with a different group velocity, the boundary of the soliton acts as a fiber-optical analog of the event horizon, preventing the escape or entry of the probe wave, which imitates the boundary of the black hole and white hole, respectively[14]. The physical mechanism underlying this process is that the intensity-dependent refractive index of the fiber (i.e., the Kerr effect) changes the group velocity of the incident probe wave, preventing it from passing through the soliton[14–16]. The change of group velocity is essentially a nonlinear frequency conversion between the incident probe wave and the newly generated DW (i.e., the idle wave), and the probe wave occurs with a blue-shift and red-shift at a white-hole and a black-hole horizon, respectively[14,17–19]. This mechanism can effectively generate ultra-broadband and coherent SC with neither soliton fission nor modulation instability[20]. The frequency conversion between the probe wave and the idle wave turns out to be reversible for both bright and dark solitons in the regime of an optical event horizon[21]. A weak DW trapped by a solitonic well consisting of a pair of temporally

separated solitons has been studied numerically and experimentally[22–24]. A probe wave with an appropriate intensity can change the trajectory of solitons and cause soliton collision or fusion[25]. However, most of the studies about the interactions between the probe wave and the soliton in the regime of an optical event horizon focus on the bright-fundamental solitons as well as dark solitons and only a few studies on high-order solitons[20–34]. Compared with dark solitons and bright-fundamental solitons, the collision dynamics between high-order solitons and probe waves can produce more interactions and richer spectral components. Especially, the polychromatic resonant radiation at the optical event horizon is unique to the interaction between the second-order soliton and the probe wave, because the second-order soliton has excellent robustness under the perturbation of moderate third-order dispersion (TOD)[10]. When the higher-order soliton ($N > 2$, N is the soliton order) interacts with the probe wave, it will be split under the perturbation of HOD. Therefore, the formation of the optical event horizon is essentially the interaction between the probe wave and the split fundamental-order soliton, so polychromatic resonant radiation will not be generated. In addition, we quantitatively discuss the interaction between the second-order soliton and the probe wave under the conditions of group velocity match (GVM) and group velocity mismatch (GVMM). By comparison, we find that the GVMM condition is more conducive to the study of the sustained and stable collision dynamics between the second-order soliton well and the probe wave. The underlying mechanism of these interactions in our study at the optical event horizon is critical for the manipulation of the soliton-probe wave dynamics.

The paper is organized as follows. In Section 2, the theoretical propagation model of the second-order soliton and the probe wave in a dispersive nonlinear optical fiber is introduced. In Section 3, the interactions between the probe wave and the second-order soliton/second-order soliton well are demonstrated and analyzed in detail. Finally, in Section 4, we summarize our numerical results.

2. Theoretical Model

The interaction between a soliton and a probe wave at the fiber-optical analog of an event horizon in a dispersive nonlinear optical fiber can be governed by the following generalized nonlinear Schrödinger equation (GNLSE)[26]:

$$i\partial_z A + \frac{1}{2}\partial_t^2 A - i\varepsilon\partial_t^3 A + |A|^2 A = 0. \tag{1}$$

Here, $z = Z/Z_0$ is the distance normalized to the dispersion length, and $t = (T - Z/v_g)/T_0$ is the time normalized to the input pulse width T_0. The dispersion length is related to second-order dispersion and pulse width as $Z_0 = T_0^2/|\beta_2|$, and v_g is the group velocity of the soliton. Here, we consider a standard single-mode fiber with a zero-dispersion wavelength (ZDW) at 1311 nm. The dispersion coefficients at the pump wavelength (1436 nm) are as follows: $\beta_2 = -14.8129\ \mathrm{ps}^2/\mathrm{km}$, $\beta_3 = 11.83\ \mathrm{ps}^3/\mathrm{km}$. The coefficient $\varepsilon = \beta_3/(6|\beta_2|T_0)$ denotes the relative intensity of TOD; here, $T_0 = 100$ fs, so $\varepsilon = 0.0133$. The non-instantaneous Raman nonlinear effect is not included here because it has a negligible impact on the dynamics at an optical event horizon[20,35]. In addition, the effects of SS and HOD (with $n > 3$) are also not included because they do not play an important role[34–36].

The input consists of a second-order soliton and a probe pulse with a temporal delay and a frequency offset, which are launched in the anomalous and normal dispersion region of the fiber, respectively. The envelope of the input field is expressed as follows:

$$A_0(t) = A_{\mathrm{Sol}}(t) + A_P(t), \tag{2}$$

where

$$A_{\mathrm{Sol}}(t) = 2\sqrt{P_0}\,\mathrm{sech}(t), \tag{3}$$

and

$$A_P(t) = A_P\,\mathrm{sech}((t - t_1)/T_1)\exp(-i\delta_P(t - t_1)). \tag{4}$$

Here, P_0 relates to the intensity of the soliton; A_P and T_1 are the amplitude and width of the probe pulse. t_1 and $\delta_P = (\omega_P - \omega_0)T_0$ are the time delay and normalized angular frequency offset between the soliton and the probe pulse. $\delta = \Delta\omega T_0 = (\omega - \omega_0)T_0$ is the normalized angular frequency offset to the second-order soliton.

3. Result and Discussion

3.1. Interaction of a second-order soliton with a probe pulse under the condition of GVM

We quantitatively discuss the interaction dynamics in the case of GVM and find that the optical event horizon is formed in this case. The wavenumber

$$D(\delta) = -\delta^2/2 + \varepsilon\delta^3 \tag{5}$$

and the group delay curves of this fiber are shown in Fig. 1(a). The GVM point in Fig. 1(a1) marked by the red dot represents a frequency offset value where the group velocities of the probe pulse and the second-order soliton are equal. The dynamics of the probe pulse is reversed on two sides of the GVM point: the GVM point is the transition point between a white-hole and a black-hole horizon. In the simulation shown in Figs. 1(b) and 1(c), the probe pulse is launched at the GVM point. Note that two pulses will never meet if their group velocities are too close to each other[35]. In our case here, although the input probe pulse is launched at the GVM point, the input ultrashort pulse has a broadband spectrum, containing many spectral components with different group velocities, which promotes the formation of the optical event horizon. As shown in Fig. 1(b), there

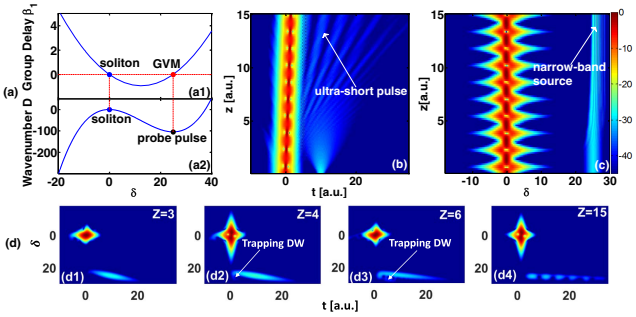

Fig. 1. (a) Wavenumber and corresponding group delay curve as a function of normalized angular frequency offset. The probe pulse is launched at a frequency offset such that the group velocities of the probe pulse and the soliton are equal. The temporal and spectral evolutions of the input field under the condition of GVM are shown in (b) and (c), respectively. (d) The corresponding spectrograms at different propagation lengths. In (b), (c), and (d), $P_0 = 1$, $A_P = 0.1$, $\delta = 25$, $t_1 = 10$, $T_1 = 3$.

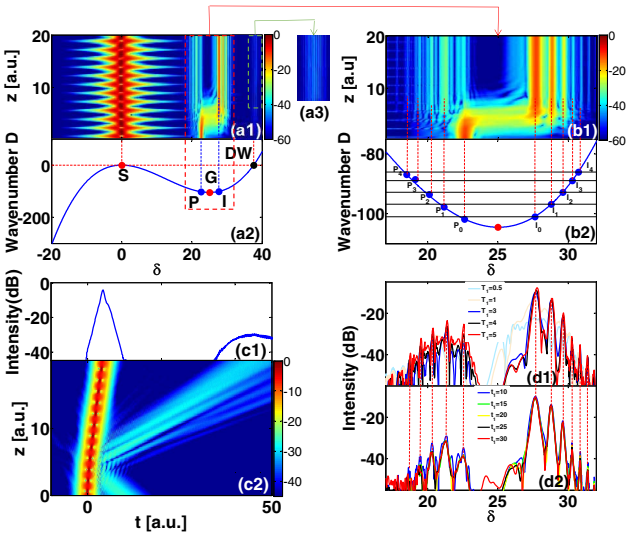

Fig. 2. (a1) Spectral and (c2) temporal evolutions of the interaction between a probe pulse and a second-order soliton under the condition of GVMM. The corresponding wavenumber curve is shown in (a2). S and P represent the launch positions of the second-order soliton and the probe pulse, respectively. DW indicates the predicted position of the dispersive wave, G stands for the GVM point, and I denotes the position of the idle wave. (a3), (b1), and (b2) are zoomed-in plots of the spectrum in the green and red boxes in (a1). The output spectrum of the oscillating radiation region when adjusting the (d1) temporal width and (d2) time delay of the incident probe pulse based on (a1). (c1) The output temporal profile. In (b2), (d1), and (d2), the vertical dashed lines indicate the locations of the pairs of the probe and idle waves, which agree with Eq. (8) quite well (as indicated by the horizontal solid lines). Here, $P_0 = 1$, $A_P = 0.1$, $\delta = 22.62$, $T_1 = 3$.

is no interaction between the second-order soliton and the probe pulse initially, until they overlap at $z = 3$. After this, the second-order soliton acts like a periodic refractive barrier, which prevents the probe pulse from passing through. Subsequently, the probe pulse is almost reflected completely from its original trajectory, while the second-order soliton still keeps its original state but with a slightly slower group velocity due to the collision with the probe pulse. When the two pulses are temporally locked due to their mutual interaction, a trapping DW indicated by the white arrow in Figs. 1(d2) and 1(d3) is generated by four-wave mixing (FWM) between the two pulses. Once the trapping DW overlaps with the probe pulse, their interference leads to a pulse with sinusoidally modulated intensity[35,37]; this process is shown in Figs. 1(d1)–1(d4). With further propagation, the temporally modulated pulse intensity leads to a correspondingly modulated refractive index profile via the Kerr nonlinearity, which produces a series of ultrashort pulses in the time domain, as shown in Fig. 1(b). Such an effect is also represented by the isolated narrow-band sources in the spectral domain in Fig. 1(c), which results from the spectral interference between the probe pulse and the trapping DW. Although the optical event horizon is formed under the condition of GVM, no distinct nonlinear frequency conversion is observed in Fig. 1(c). This is due to the fact that all the spectral components of the probe pulse are tightly enclosed around the GVM point, so the generated idle pulse almost overlaps with the probe pulse in frequency. This process imitates the phenomenon of a white-hole horizon, so all the narrow-band sources moderately move toward the high-frequency region.

3.2. Interaction of a second-order soliton with a probe pulse under the condition of GVMM

We quantitatively discuss the interaction dynamics in the case of GVMM, and some interesting phenomena have been discovered. The group velocity of the probe pulse is slightly larger than that of the second-order soliton, so the second-order soliton precedes the probe pulse temporally, as shown in Fig. 2(c2); the corresponding output temporal profile is shown in Fig. 2(c1). Some new frequency components are generated during the spectrum evolution in Fig. 2(a1). The rightmost frequency component around $\delta = 40$ composed of multiple peaks [enlarged in Fig. 2(a3)] is the Cherenkov radiation from the second-order soliton, because the central frequency of the multiple-peak structure agrees with the prediction of the DW by both phase-matching theory[26] and wavenumber curve in Fig. 1, marked by the black dot in Fig. 2(a2). Besides, the multiple-peak structure is generated before the interaction between the probe wave and the second-order soliton. So, we can conclude that the multiple-peak structure is DW emitted by the second-order soliton. The separation between the frequency peaks of the multiple-peak Cherenkov radiation is described by[10]

$$\frac{1}{2}\beta_2\delta^2 + \frac{1}{6}\beta_3\delta^3 - \tau_g\delta = \frac{1}{2}\frac{|\beta_2|}{T_0} + \frac{2\pi}{Z_s}N. \tag{6}$$

Here, Z_s is the oscillation period of the second-order soliton, N is an integer number, and $\tau_g = v_g^{-1}$ is the soliton group delay. During this interaction, the second-order soliton has excellent robustness under the perturbation of moderate TOD. So, the

resonance frequencies for the radiation generated by cascaded FWM between the probe pulse and the second-order soliton can be derived via the perturbation theory used for fundamental solitons[26,35]. This theory indicates that the probe pulse experiences a nonlinear optical frequency conversion to an idler, which satisfies the following resonance condition[26]:

$$D(\omega_P - \omega_0) = D(\omega_I - \omega_0). \tag{7}$$

As shown in Fig. 2(a1), the resonant radiation is polychromatic owing to the unequally spaced narrow-band sources generated by frequency modulation. This is in contrast to the case of fundamental solitons, where the resonant radiation only has one frequency peak. While there are five probe and idle pairs shown in Fig. 2(b1), as can be seen from Fig. 2(b2), they all satisfy the wavenumber-matching relationship. So, we can draw the following conclusion:

$$D(\omega_{P_n} - \omega_0) = D(\omega_{I_n} - \omega_0). \tag{8}$$

This phenomenon can be understood as follows. When the probe pulse collides with the second-order soliton, it turns into a series of narrow-band sources under the effect of cascaded FWM; at the same time, the idle wave with corresponding resonant peaks is generated via the wavenumber-matching relationship. Adjusting the width of the probe pulse changes the output spectrum of the oscillating radiation, as shown in Fig. 2(d1). Interestingly, the spectral peaks of the output spectrum seem to be independent of the probe pulse width when the probe pulse is wide enough, since both the phase-matching condition and the regular evolution of second-order solitons have not changed. The frequency peaks for $T_1 = 3$, $T_1 = 4$, as well as $T_1 = 5$ almost overlap. However, no obvious probe and idle pairs are found for a width of the probe pulse narrower than 3. This is because decreasing the width of the incident probe pulse raises the time interval between the incident probe pulse and the trapping DW. Here, the trapping DW is generated by the same mechanism as in the case of GVM. The time interval is inversely proportional to the modulation frequency. So, the spectral width of the narrow-band sources slightly reduces, and the pairs of probe and idle waves overlap in frequency and modulate with each other. When we moderately regulate the time delay of the probe wave, the frequency positions of the probe and idle pairs do not change, as shown in Fig. 2(d2). This is because the time intervals between the probe waves and the trapping DWs are unchanged. In addition, we can see from Figs. 2(d1) and 2(d2) that most of the energy of the probe wave has been converted to an idle wave. The energy conversion efficiency is slightly affected by the pulse width and time delay of the probe wave. So, we can conclude from the above discussion that when the temporal width of the probe pulse is large enough, it is convenient to observe the nonlinear frequency conversion between the polychromatic probe and idle waves under the condition of GVMM.

3.3. Manipulation of a soliton well by a weak probe pulse

In this section, we focus on the dynamics between the soliton well and the probe wave under the condition of GVMM. The soliton well is composed of two identical second-order solitons separated in time. An incident envelope consisting of a second-order soliton well and a weak probe pulse at the corresponding GVMM point can be mathematically expressed as follows:

$$\begin{aligned} A(t=0) = {} & A_P \operatorname{sech}(t/T_1) \exp(-i\delta_P t) \\ & + 2\sqrt{P_0} \operatorname{sech}(t - t_1) \\ & + 2\sqrt{P_0} \operatorname{sech}(t + t_1). \end{aligned} \tag{9}$$

The simulated collision dynamics of the probe pulse with the pair of second-order solitons (i.e., a soliton well) is shown in Fig. 3. In Figs. 3(a1) and 3(a2), the parameters are identical with those used in Fig. 2(a1). As shown here, the probe pulse initially bounces back and forth within the soliton well. The soliton well plays the role of temporal analog of a planar dielectric multimode waveguide, including limited support modes. After several collisions, the probe pulse begins to escape from the soliton well. This is because the temporal analog of the multimode waveguide structure breaks down as a result of the split of second-order solitons, which leads to the decline of the constraint ability of the soliton well. Pairs of main solitons (high intensity) and fissioned solitons (low intensity) are generated by the probe-pulse-induced soliton fission, which obtains a red and blue frequency shift. The collision between the two main solitons shown in Fig. 3(a1) at $z = 33.5$ is induced by the effective interaction force acting as the effective attraction owing to multiple scatterings with the probe pulse. The collision-induced DW (CDW) is scattered at a frequency determined by the standard phase-matching

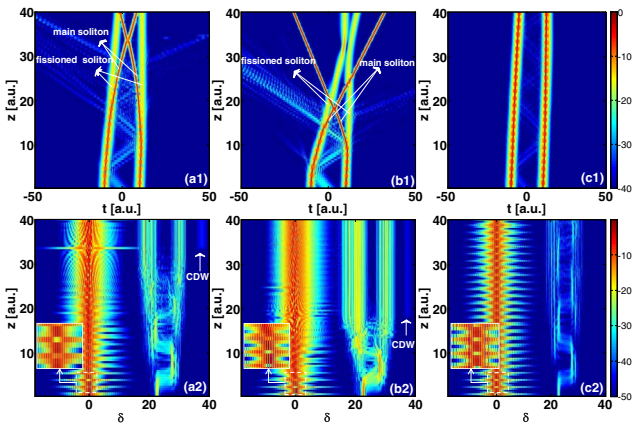

Fig. 3. (a1)–(c1) The temporal and (a2)–(c2) spectral evolutions of the collision process between two well-separated second-order solitons and a probe pulse with different amplitudes A_P: (a) 0.1, (b) 0.2, (c) 0.05. The white boxes are the partial enlargement of the corresponding white dotted boxes. Here, the other parameters of the simulation are the same as those used in Figs. 2(a1) and 2(c).

condition, where the peak power and central frequency are the four solitons superposition field attained during the collision and the mean frequency of the nonlinear superposition, respectively[23]. No DW is scattered before or after the collision by the individual main solitons because the frequency offset of the two solitons from the ZDW is too large to satisfy the phase-matching condition for DW generation. During the collision, it precisely affects both the bandwidth and peak power that allows the phase-matching condition for DW generation to be satisfied.

When doubling the amplitude of the probe pulse ($A_P = 0.2$), not only the two main solitons but also the two fissioned solitons collide, as shown in Fig. 3(b1). However, no obvious CDW is generated by the collision of the two fissioned solitons owing to their low intensities. Increasing the amplitude of the probe pulse from 0.1 to 0.2 advances the collision position of the two main solitons from $z = 33.5$ to $z = 18$. This is because the effective attraction is proportional to the intensity of the input probe pulse, and, in turn, the greater the power of the input probe pulse, the greater the absolute time delay of the two solitons and the closer the two solitons, the shorter the distance where solitons collision occurs. On the contrary, the probe pulse can bounce within the soliton well for a longer distance, while the two second-order solitons can maintain their original trajectories by decreasing the amplitude of the probe pulse to 0.05 [Figs. 3(c1) and 3(c2)]. The trapping efficiency, defined as the ratio of the energy confined in the soliton well to the energy of the initial probe pulse, is higher than the previous two cases shown in Figs. 3(a1) and 3(b1). In all cases, the time-domain asymmetry of the soliton well in Figs. 3(a1), 3(b1), and 3(c1) is caused by the collision of the probe wave with the soliton well and the perturbation of TOD.

Another obvious phenomenon is that the sinusoidally modulated power spectrum in the frequency domain is caused by a pair of second-order solitons with a fixed phase relationship, which can be seen in the enlarged figures in Figs. 3(a2), 3(b2), and 3(c2). The phase between two second-order solitons can be controlled by their time delay, and the oscillation period of the sinusoidally modulated spectrum is inversely proportional to the time delay. So, the interference fringes are extremely narrow near $z = 0$. As the two main solitons and two fission solitons are close to each other, the interference fringes gradually widen. The spectral oscillation period is the largest at the collision point of two main solitons. After the collision, the two main solitons move farther away, leading to a decreasing period of the interference fringes.

To further investigate the collision dynamics between the soliton well and a probe pulse in an optical event horizon, we plot the dependence of the collision position (Z_c) of the two main solitons on the amplitude and width of the probe pulse in Fig. 4. The width of the probe pulse is fixed at $T_1 = 3$ in Fig. 4(a). As shown here, increasing the amplitude of the probe pulse decreases the value of Z_c. The increasing amplitude of the probe pulse enhances the effective attraction between the solitons, which accelerates the splitting of the solitons and the collision of the two main solitons. Figure 4(b) shows that the

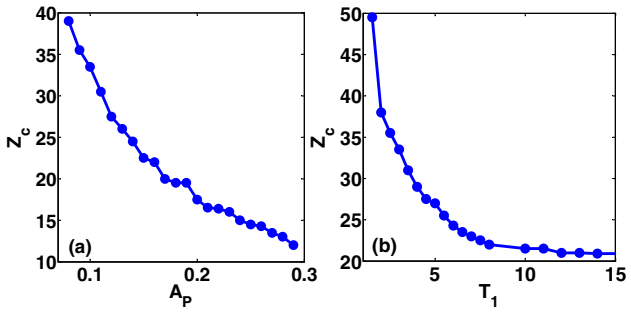

Fig. 4. Collision distance of the two main solitons, Z_c, as a function of (a) the amplitude A_P and (b) the temporal width T_1 of the incident probe pulse. The width of the probe pulse is fixed at $T_1 = 3$ in (a), while the amplitude of the probe pulse is fixed at $A_P = 0.1$ in (b).

collision distance (Z_c) can be regulated by adjusting the width of the probe pulse. Here, the amplitude of the probe pulse is fixed to $A_P = 0.1$. Increasing the width of the probe pulse narrows its spectral width and reduces its broadening speed in time, which helps to maintain the intensity of the probe pulse. This effectively decreases the value of Z_c. So, we can conclude from Fig. 4 that regulating the amplitude and width of the probe pulse is two effective ways to control the collision dynamics of a soliton well in an optical event horizon.

4. Conclusion

In conclusion, we propose an approach to actively control the interaction of the second-order soliton with an external probe pulse under the condition of GVM and GVMM. In both cases, an optical event horizon is formed, and the probe pulse becomes a series of narrow-band sources with adjustable spectrum width, which represent as ultrashort pulses with various widths in time. Especially in the case of GVMM, all the spectral components of narrow-band sources follow the frequency conversion relationship according to the wavenumber-matching relationship, as well as the multiple-peaks Cherenkov radiation from two solitons at the predicted position with the regular interval. By comparison, the probe pulse under the case of GVMM is more favorable to investigate the collision dynamics of soliton wells. We further studied the case of a probe pulse with a soliton well consisting of two second-order solitons. We find abundant collision dynamics, where the collision location can be adjusted via the width and intensity of the probe pulse. In addition, CDW is observed by the collision of two energetic fundamental solitons split from the second-order solitons, which enriches the spectrum components. Therefore, the collision dynamics of a soliton well can be well controlled by the probe pulse. The dynamics in the optical event horizon provides a fundamental explanation of frequency conversion and broadband light generation in nonlinear optical waveguides, which allow us to better understand the fiber-optical analog of the event horizon and pave the way for the on-chip application.

Acknowledgement

This work was supported by the National Key Research and Development Program of China (No. 2018YFB0704000), the Open Fund of the State Key Laboratory of Integrated Optoelectronics (No. IOSKL2020KF20), and the National Natural Science Foundation of China (No. 61275137).

References

1. G. P. Agrawal, *Nonlinear Fiber Optics*, 4th ed. (Academic Press, 2007).
2. F. Köttig, F. Tani, J. C. Travers, and P. S. J. Russell, "PHz-wide spectral interference through coherent plasma-induced fission of higher-order solitons," Phys. Rev. Lett. **118**, 263902 (2017).
3. M. Selim Habib, C. Markos, O. Bang, and M. Bache, "Soliton-plasma nonlinear dynamics in mid-IR gas-filled hollow-core fibers," Opt. Lett. **42**, 2232 (2017).
4. Y. S. Kivshar and V. Agrawal, *Optical Solitons: From Fibers to Photonic Crystals* (Academic Press, 2003).
5. I. Cristiani, R. Tediosi, L. Tartara, and V. Degiorgio, "Dispersive wave generation by solitons in microstructured optical fibers," Opt. Express **12**, 124 (2004).
6. J. Rong, H. Yang, and Y. Xiao, "Accurately shaping supercontinuum spectrum via cascaded PCF," Sensors **20**, 2478 (2020).
7. R. Driben, B. A. Malomed, A. V. Yulin, and D. V. Skryabin, "Newton's cradles in optics: from N-soliton fission to soliton chains," Phys. Rev. A **87**, 063808 (2013).
8. F. Braud, M. Conforti, A. Cassez, A. Mussot, and A. Kudlinski, "Solitonization of a dispersive wave," Opt. Lett. **41**, 1412 (2016).
9. A. Antikainen, F. R. Arteaga-Sierra, and G. P. Agrawal, "Temporal reflection as a spectral-broadening mechanism in dual-pumped dispersion-decreasing fibers and its connection to dispersive waves," Phys. Rev. A **95**, 033813 (2017).
10. R. Driben, A. V. Yulin, and A. Efimov, "Resonant radiation from oscillating higher order solitons," Opt. Express **23**, 19112 (2015).
11. S. L. Zhao, H. Yang, Y. Huang, and Y. Z. Xiao, "Generation of tunable ultrashort pulse sequences in a quasi-discrete spectral supercontinuum by dark solitons," Opt. Express **27**, 23539 (2019).
12. L. H. Zhu, Z. J. Zheng, X. G. Ge, and G. G. Du, "High-power, ultra-broadband supercontinuum source based upon 1/1.5 μm dual-band pumping," Chin. Opt. Lett. **19**, 041403 (2021).
13. W. Wang, H. Yang, P. Tang, C. Zhao, and J. Gao, "Soliton trapping of dispersive waves in photonic crystal fiber with two zero dispersive wavelengths," Opt. Express **21**, 11215 (2013).
14. T. G. Philbin, C. Kuklewicz, S. Robertson, S. Hill, F. König, and U. Leonhardt, "Fiber-optical analog of the event horizon," Science **319**, 1367 (2008).
15. D. Faccio, "Laser pulse analogues for gravity and analogue Hawking radiation," Contemp. Phys. **53**, 97 (2012).
16. F. Belgiorno, S. L. Cacciatori, M. Clerici, V. Gorini, G. Ortenzi, L. Rizzi, E. Rubino, V. G. Sala, and D. Faccio, "Hawking radiation from ultrashort laser pulse filaments," Phys. Rev. Lett. **105**, 203901 (2010).
17. S. Robertson and U. Leonhardt, "Frequency shifting at fiber-optical event horizons: the effect of Raman deceleration," Phys. Rev. A **81**, 063835 (2010).
18. A. Choudhary and F. König, "Efficient frequency shifting of dispersive waves at solitons," Opt. Express **20**, 5538 (2012).
19. O. Melchert, C. Bree, A. Tajalli, A. Pape, and R. Arkhipov, "All-optical supercontinuum switching," Commun. Phys. **3**, 146 (2020).
20. A. Demircan, S. Amiranashvili, C. Brée, and G. Steinmeyer, "Compressible octave spanning supercontinuum generation by two-pulse collisions," Phys. Rev. Lett **110**, 233901 (2013).
21. Z. Deng, X. Shi, C. Tan, and X. Fu, "Reversible conversion between optical frequencies of probe and idler waves in regime of optical event horizon," J. Opt. Soc. Am. B **33**, 857 (2016).
22. A. V. Yulin, R. Driben, B. A. Malomed, and D. V. Skryabin, "Soliton interaction mediated by cascaded four wave mixing with dispersive waves," Opt. Express **21**, 14481 (2013).
23. Z. Deng, X. Fu, J. Liu, C. Zhao, and S. Wen, "Trapping and controlling the dispersive wave within a solitonic well," Opt. Express **24**, 10302 (2016).
24. S. F. Wang, A. Mussot, M. Conforti, X. L. Zeng, and A. Kudlinski, "Bouncing of a dispersive wave in a solitonic cage," Opt. Lett. **40**, 3320 (2015).
25. R. Driben and I. V. Babushkin, "Accelerated rogue waves generated by soliton fusion at the advanced stage of supercontinuum formation in photonic-crystal fibers," Opt. Lett. **37**, 5157 (2012).
26. D. V. Skryabin and A. V. Yulin, "Theory of generation of new frequencies by mixing of solitons and dispersive waves in optical fibers," Phys. Rev. E. **72**, 016619 (2005).
27. A. G. Mahmoud, B. Toshihiko, E. Manfred, and Y. P. Alexander, "Front-induced transitions," Nat. Photonics **13**, 737 (2019).
28. A. Mahalingam and K. Porsezian, "Propagation of dark solitons with higher-order effects in optical fibers," Phys. Rev. E **64**, 046608 (2001).
29. C. Milián, D. V. Skryabin, and A. Ferrando, "Continuum generation by dark solitons," Opt. Lett. **34**, 2096 (2009).
30. T. Marest, C. Mas Arabí, M. Conforti, A. Mussot, C. Milián, D. V. Skryabin, and A. Kudlinski, "Emission of dispersive waves from a train of dark solitons in optical fibers," Opt. Lett. **41**, 2454 (2016).
31. T. Marest, C. M. Arabí, M. Conforti, A. Mussot, C. Miliín, D. V. Skryabin, and A. Kudlinski, "Grayness- dependent emission of dispersive waves from dark solitons in optical fibers," Opt. Lett. **43**, 1511 (2018).
32. J. F. Rong, H. Yang, Y. Z. Xiao, and Y. F. Chen, "Mutual manipulation between dark soliton and probe wave for the gray-dark solitonic well," Phys. Rev. A **103**, 023505 (2021).
33. Z. X. Deng, J. Liu, X. W. Huang, C. J. Zhao, and X. L. Wang, "Active control of adiabatic soliton fission by external dispersive wave at optical event horizon," Opt. Express **25**, 28556 (2017).
34. W. Y. Cai, Y. Y. Tian, L. F. Zhang, H. R. He, J. J. Zhao, and J. Wan, "Reflection and refraction of an airy pulse at a moving temporal boundary," Annalen der Physik **532**, 2000295 (2020).
35. K. E. Webb, M. Erkintalo, Y. Xu, N. G. Broderick, J. M. Dudley, G. Genty, and S. G. Murdoch, "Nonlinear optics of fibre event horizons," Nat. Commun. **5**, 4969 (2014).
36. C. M. Arabí, F. Bessin, A. Kudlinski, A. Mussot, D. Skryabin, and M. Conforti, "Efficiency of four-wave mixing between orthogonally polarized linear waves and solitons in a birefringent fiber," Phys. Rev. A **94**, 063847 (2016).
37. E. Rothenberg, "Colliding visible picosecond pulses in optical fibers," Opt. Lett. **15**, 443 (1990).